

Article

Decentralized Power Management for Electrical Power Systems in More Electric Aircrafts

Myungchin Kim ¹, Sung Gu Lee ² and Sungwoo Bae ^{3,*} ¹ School of Electrical Engineering, Chungbuk National University, Cheongju 28644, Korea; mckim@cbnu.ac.kr² Electronic Robot Engineering, Busan University of Foreign Studies, Busan 46234, Korea; sunggu@bufs.ac.kr³ Department of Electrical Engineering, Hanyang University, Seoul 04763, Korea

* Correspondence: swbae@hanyang.ac.kr; Tel.: +82-2-2220-2309

Received: 17 July 2018; Accepted: 7 September 2018; Published: 10 September 2018



Abstract: In order to implement reliable and flexible power management among energy sources, a decentralized power management approach for electrical power systems (EPSs) in the more electric aircraft (MEA) is studied. Considering the increased use of electrical power for various functions, the performance of MEA would be determined by the design and operation of the EPS. By using a virtual impedance that includes both a resistive term and an inductive term, autonomous power sharing is realized. Because of the frequency dependence in the virtual impedance, different power sharing ratios between steady state and transient state can be considered. Not only the operation of various power sources is coordinated without supervision of a centralized controller, but also the operation profile of each source can be adjusted to meet output characteristics of each source. To demonstrate the effectiveness of the proposed approach, a series of simulations that consider various virtual impedance configurations were conducted. The proposed approach contributes to a higher level of operational flexibility, while enabling reliable and cost-effective management of MEAs.

Keywords: DC micro-grid; virtual impedance; virtual inductance; more electric aircraft

1. Introduction

This paper studies a decentralized approach for electrical power systems (EPS) management in more electric aircraft (MEA) platforms. Similar to vehicular platforms for ground [1] and marine [2] transportation, research on highly electrified aircrafts has received continuous interest. As a result of aircraft electrification, the roles of EPSs have broadened from relatively simple functions to essential functions such as propulsion and flight control [3]. For instance, electrical motors are used for actuation of flight control surfaces [4,5] and aircrafts that use a pure electric or a hybrid electric propulsion architecture have been developed [6,7].

Major motivations for aircraft electrification include social demand toward sustainable transportation and improved flight performance. While combustion engines have been used as the primary source for propulsion in conventional aircrafts [8], platforms that utilize renewable sources to generate propulsion force have been developed [6,9]. By replacing massive hydraulic/mechanical actuation systems with electrical actuators, it is possible to improve performance by weight reduction and efficiency improvement [10]. Thanks to the recent development of electrical motors and power electronic interfaces with high power density, platform electrification is being considered not only for small sized quad-copters (drones) but also for manned aircrafts. In Figure 1, examples of electrical loads used in conventional aircrafts and the MEA are illustrated [3,4,8]. Although the use of electrical interfaces seems to introduce potential advantages compared to conventional aircrafts, electrified aircrafts should also satisfy safety and reliability regulations as in current platforms.

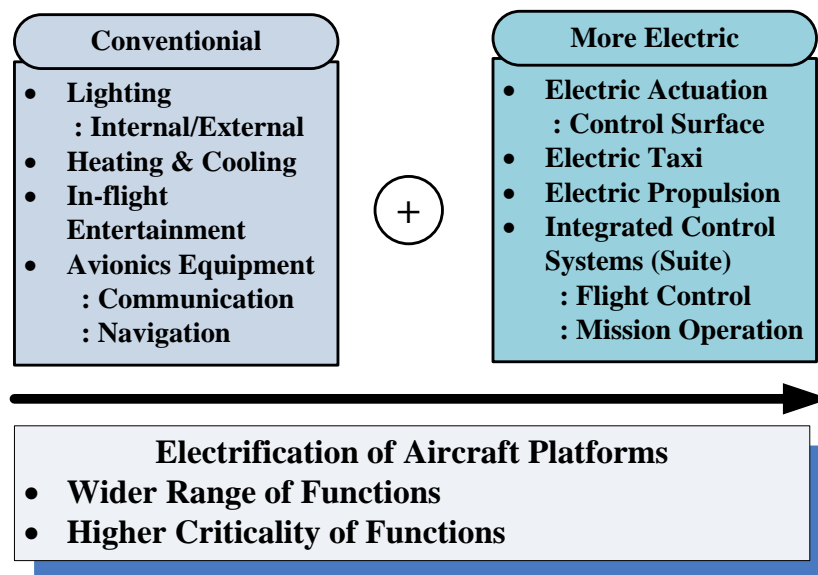


Figure 1. Increased use of electrical power in a more electric aircraft (MEA).

Figure 2 shows a generalized architecture of an EPS in MEA applications. As shown in Figure 2, the EPS consists of various type of sources, loads and energy storage. Considering the growing interest for the MEA, research on both the EPS itself and the EPS components is required. While 115 V/400 Hz ac and 28 V dc system buses have been considered for electrical distribution in conventional aircrafts [8], 270 V dc-based systems have been developed in recent aircrafts [8,9]. In addition to the voltage levels, research on EPS architecture has also been performed. Examples of architectures include ac systems with constant [8] or variable frequency [10], dc systems [9] and hybrid ac/dc [11] systems. While the EPS architecture should be selected based on a comprehensive review of various factors, it has been reported that selecting 270 V dc for power distribution seems to be a promising option from the perspective of weight and stability [9]. In such an EPS, the power is transferred to the load using dc distribution, while the interface requirements of 28 V dc or ac loads are met by using power electronic interfaces. In order to design an EPS that meets various system level requirements (e.g., power quality, efficiency, and weight), optimization studies on the overall EPS architecture [9], subsystems and components [12] have also been performed.

Increased use of power electronic interfaces and various power sources in aircraft platforms has raised needs for research on control of dc and ac/dc hybrid power networks. While power electronic interfaces enable flexible design and operation of power systems, the performance (e.g., stability, dynamic response and effective protection) of the overall system is highly affected by the system control approach [13–15]. In order to perform power sharing in a decentralized manner, it is general to apply droop-based approaches [15]. In case the droop is implemented by a virtual resistance, the resistance value determines the power sharing ratio among power sources [14,15]. Through a stability analysis, it has been reported that the stability characteristics of droop-controlled dc microgrids are highly affected by system parameters, such as the cable resistance and load type [16]. Although the virtual resistance enables autonomous control, the desired power sharing ratio can be achieved only at steady state. Instead, droop-based approaches that manage power sharing during transients have been studied. For example, Reference [17] introduces how low pass filters and high pass filters can be incorporated with the virtual resistance to design the power sharing performance during transient periods. In [18,19], a virtual capacitance is used to manage the power sharing performance during transients. It was demonstrated that the power output of sources during transients is affected by the filter characteristics or the type of virtual impedance (e.g., resistive or capacitive). Control approaches that contribute to modular operation [13] or minimized power oscillations [20] in hybrid ac/dc systems have also been studied. While the approach of [13] performs system control without requiring full

information of the system by a nonlinear observer, the study of [20] improves the transient response characteristics by a neural network based damping controller.

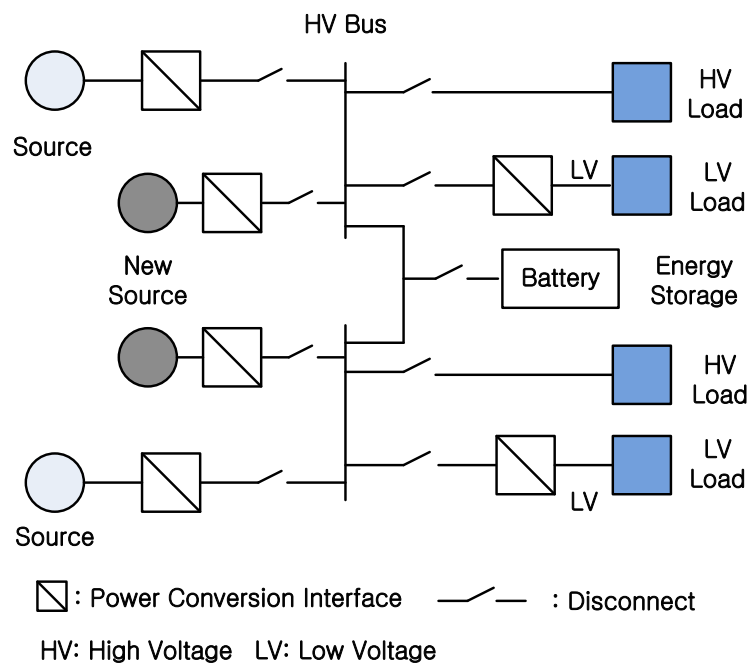


Figure 2. Configuration of a generalized EPS in an MEA.

With the increased use of renewable power sources and electrical loads, power management of EPS has become critical to ensure reliable power supply for loads in MEAs. Similar to stationary microgrids that consist of various renewable sources [21], energy management systems for EPS in airborne platforms have also been studied [22,23]. In order to maintain instantaneous power balance between sources and loads, not only the output of each source should be effectively controlled [21] but coordination among power sources is also required [7]. For example, an EPS that consists of proton exchange membrane fuel cell (PEMFC), photovoltaics (PV) and battery have been considered for an unmanned aircraft [24]. As the power demand varies depending on the flight maneuver pattern, the output of the PEMFC and PV cells are adjusted according to the instantaneous load demand such that various flight patterns could be performed and the battery state-of-charge (SOC) level could be maintained above a pre-defined level throughout the flight. It is worth noting that energy storage (e.g., battery) is a critical component in aircrafts as it operates as a back-up source when primary power sources are not operational. When the main propulsion has failed, the battery SOC level would determine the available flight period for an aircraft to make necessary maneuvers for landing or recovery in emergency situations. Even during normal flight conditions, the battery can be discharged to handle rapid increase of power demand that can occur during dynamic maneuvers.

As the operation mode of each load and the connection status of each disconnect of Figure 2 could be different depending on each mission phase of the overall flight, the system control should effectively respond to configuration changes. In particular, the EPS should be able to handle various abnormal conditions that could be caused by faults or load conditions. In case a fault occurs, the power flow of the EPS should be reconfigured so that the fault is locally isolated, and the rest of the EPS is not affected. As the system response differs for each fault case, a comprehensive fault analysis should be conducted. Fault analysis approaches that provide insights on the system behaviors to unsymmetrical faults have been proposed and the response characteristics for various scenarios have been studied using fault models of various distributed energy sources [25,26]. Considering the increased connection of loads in MEA, the effect of constant power loads to dc systems [27] and unbalanced loads to ac microgrids [28] have been studied.

Meanwhile, researches on design approaches for improved performance of power electronic interfaces in MEA applications have been performed. While researches on control approaches [29] and fault tolerant drive systems [30] have been conducted, design for highly reliable operation [31] and increased power density [32] have received attention for aerospace applications. In order to address needs for weight reduction and meeting requirements of design standards, in particular, studies on performance analysis [33] and optimization [34] of electromagnetic interference (EMI) filters have been actively performed. The main direction for power converters is to achieve a high-power density so that the overall aircraft weight could be reduced [4,35].

In this manuscript, an approach that realizes decentralized power management of EPS in the MEA is introduced. Instead of receiving power commands from a central control unit [36], the command for each source is generated based on the data that are measured from the terminal. Despite the growing interest for MEA, there seems to be limited research on decentralized control approaches of EPS in aircrafts [22,23]. In fact, EPS in most conventional aircrafts has been designed such that each distribution bus is connected to a single generator instead of connecting multiple generators in parallel [37]. With the increased use of multiple sources in MEA, however, it is necessary to study approaches that enable decentralized modular control without violating conventional reliability requirements of the aircraft. Moreover, this paper demonstrates how the virtual impedance could be effectively used to achieve a desired power sharing ratio. The power sharing ratios at steady state and transient state are adjusted separately by designing the virtual resistance and the virtual inductance. Hence, the power flow can be controlled in a more flexible manner. Detailed explanation on the contributions of the presented work are introduced in the following section.

The rest of the paper is as follows: Section 2 highlights the detailed contributions of the manuscript, while Section 3 introduces the decentralized power control approach for MEAs. Section 4 demonstrates the performance of the considered control approach and the final section concludes the paper.

2. Contributions of Present Work

Detailed explanation on how the current research contributes to effective decentralized control of EPS in MEA platforms are as follows.

First, the proposed approach enables autonomous control of EPS in MEA platforms. The application of decentralized control could achieve reliable operation compared to centralized control architectures [38,39]. Because of the decentralized nature, for example, system failures caused by faults in the communication interface could be prevented. Hence, the EPS can be controlled in a fault tolerant manner [38]. Considering the catastrophic consequences of system failure, the importance of system reliability should not be underestimated for aircrafts. Especially, EPS reliability would be a critical factor that determines the overall platform safety because of the increased use of electrical power in highly electrified aircrafts. Although system reliability depends not only on the component reliability but also the system control architecture, prior researches on EPSs of MEAs have been limited to topics such as electrical actuator performance [4] and stability analysis [11]. While approaches for improved reliability have been studied [31,40], such studies have focused on the power interface and not on the overall EPS. Although control laws for MEA EPSs have been discussed, the work of this paper differs by considering a decentralized architecture [22] or considering performance during transient periods [41].

Second, this paper demonstrates that the power sharing ratio among various sources can be controlled to be different between steady state and transient periods. Such increased flexibility in power flow control would contribute to effective operation of MEA so that each power source could be operated according to their inherent output characteristics (i.e., energy density and power density). Figure 3 compares the typical values of energy density and power density for common power sources [42,43]. For example, the output of sources with high power density could be operated to supply high peak power during short transients and limited power at steady state. In case of sources that have high energy densities, a reversed operation profile could be considered.

While the supercapacitor has been used as a representative energy storage that handles transient power imbalances, the fuel cell has been considered in aircraft applications as a source with relatively large energy density [7]. While the application of PEMFC and solid oxide fuel cells (SOFC) has been reported for aircrafts [7], PEMFC have been mostly used thanks to its superior properties in power density, operation temperature and efficiency [7,44]. As each source could be controlled in a more flexible manner, the output of each source could be coordinated to achieve optimized operation of the overall EPS. While most previous studies on decentralized power control (i.e., droop control) have focused on improving the power sharing performance at steady state [38,45,46], the focus of this paper is on using the virtual impedance to enable flexible power sharing for both steady state and transients throughout the overall flight profile. Indeed, research on improving dc microgrid performance during transient periods have been performed [17–19,47]. Instead of using virtual capacitors [18,19] or the first order filters [17], however, this paper studies the application of virtual inductors. While a virtual inductance was used in [47], the focus of such research was on decreasing power oscillations instead of realizing flexible power sharing. Compared to virtual impedances that are either purely inductive [47] or capacitive [18,19], in addition, this research explores the effective usage of virtual impedances that include both a resistive term and an inductive term. By including a resistive component, the corresponding source can participate in power sharing for both steady state and transient conditions.

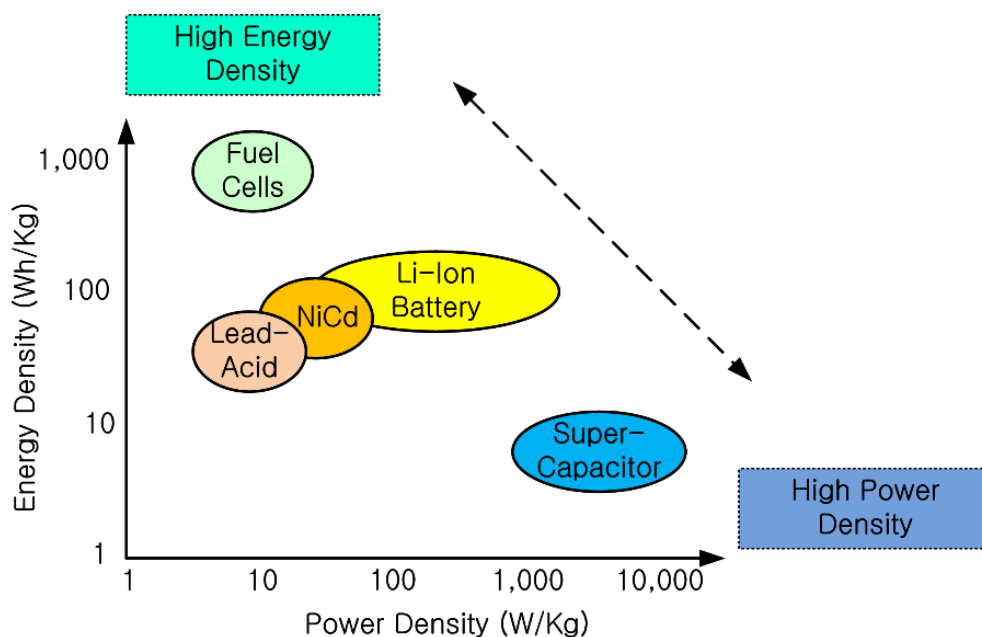


Figure 3. Comparison of power source characteristics (Redrawn using data of [42,43]).

Third, practical challenges that occur during realistic operation of aircraft EPS are addressed. Especially, the needs for minimal impact caused by changes in the EPS configuration are considered. Thanks to the decentralized control architecture of the considered approach, removal and addition of components could be performed in a modular fashion compared to centralized approaches [13]. Such modularity enables aircraft retrofit tasks to be performed with minimal efforts. With the continuous development of advanced electronic payloads [8], system control approaches should support activities of system modification and equipment replacement in a simpler way. As the burden that each power source should handle at steady state and transients could be set to be different, in addition, the considered virtual impedance-based approach enables system operation so that the lifetime of the power sources could be maximized. As reported in detailed lifetime studies [48,49], the aging of fuel cells and batteries are determined by the operation profiles of each source. For example,

fuel cells show expedited aging when it experiences large power transients [48] and the operation profile has direct impact on the thermal stress of batteries [49].

3. Decentralized Power Management for an MEA EPS

3.1. Limitations of Centralized Power Management

For a MEA EPS, system control can be performed by either a centralized [36] or a decentralized [38] architecture. In case of the centralized approach, as shown in Figure 4, the central power control unit (PCU) generates command values for each power source. As the detailed information of the overall EPS is transferred to the PCU, integrated information can be provided to the system operator (i.e., pilot of manned aircrafts or ground station control personal of unmanned aircrafts) for increased situational awareness. Based on the monitored data of the EPS, necessary corrective action could be performed by the system operator to handle abnormal operation situations such as emergency or faults. Furthermore, optimized operation of the EPS could be performed using the feedback information of the overall EPS.

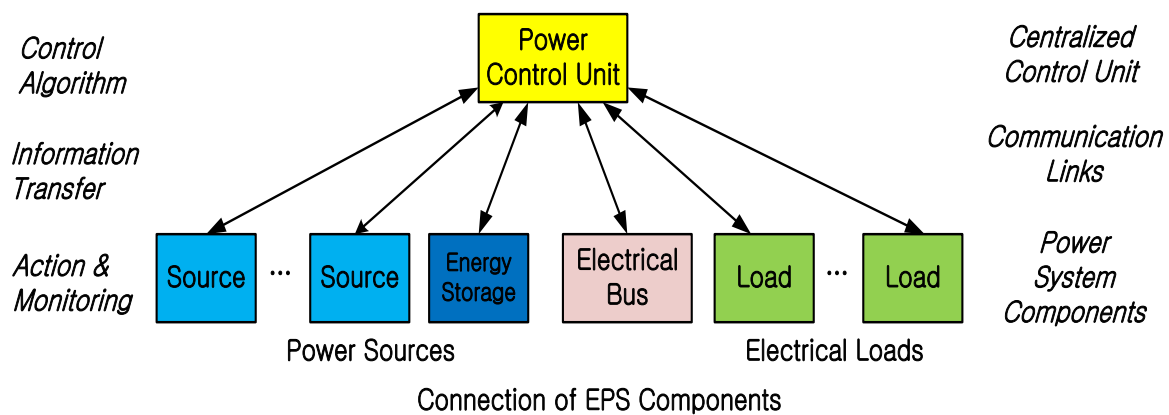


Figure 4. Centralized control architecture for an aircraft EPS.

Although the centralized approach realizes integrated power management, the operation of the EPS depends on the communication link reliability. In case feedback of the necessary information from components is unavailable because of faults in the communication path, the performance of the PCU would also be affected. In case it is assumed that the PCU and EPS components are fully operational, the reliability of the overall EPS can be expressed as

$$R_{EPS}(t) = \prod_{i=1}^M R_i(t) \tag{1}$$

where M is the total number of EPS components and $R_i(t)$ is the reliability of the communication link between the PCU and the i th EPS component. Assuming a constant failure rate, the reliability of each communication link can be written as [50]

$$R(t) = e^{-\lambda t} \tag{2}$$

where λ is the failure rate of the communication link. Figure 5 shows how the reliability of the EPS at 1000 h varies as the number of EPS component (M) increases. In order to study the effect of different failure rates, the failure rate of $\lambda_1 = 2$ failures/ 10^6 h, $\lambda_2 = 5$ failures/ 10^6 h, and $\lambda_3 = 10$ failures/ 10^6 h were considered. As shown in Figure 5, the reliability of the overall EPS decreases as the number of EPS components increase, regardless of the failure rate value. That is, the reliability of the centralized power management approach depends not only on the reliability of the component itself but also on the status of the communication link. Hence, it is necessary to develop a decentralized control

architecture that performs effective power management in an EPS for the MEA to achieve higher system reliability.

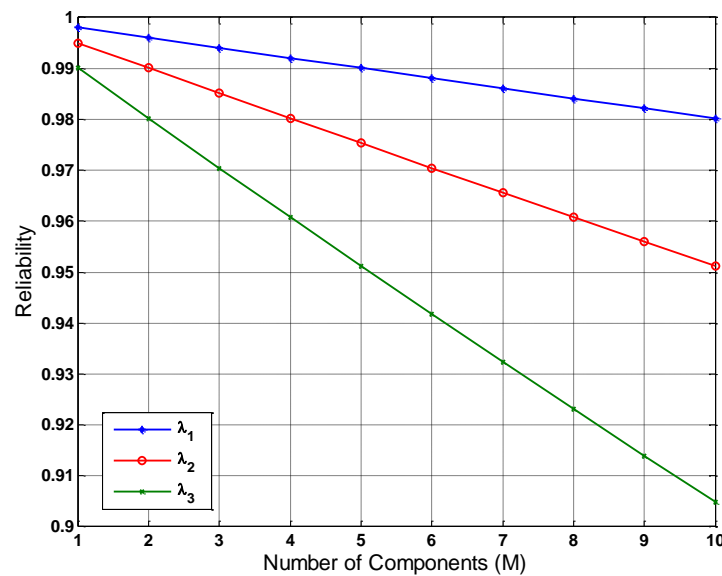


Figure 5. System reliability with different failure rates and number of components.

3.2. Decentralized Power Management

In order to realize decentralized power management, this research uses the virtual impedance to determine the power sharing ratio among different power sources. Figure 6 shows the block diagram of the considered approach. As shown in Figure 6, the controller has a cascaded configuration that relies on the feedback of both the voltage and the current. The control output is converted to a sequence of switching signals using pulse-width modulation (PWM) [51]. The virtual impedance is used when the reference value for the voltage controller is generated as

$$v_i^* = V_0 - Z_v \cdot i_o \tag{3}$$

where V_0 is the no-load voltage, Z_v is the virtual impedance, and i_o is the output current of the power source. As the command value for the voltage controller is generated by subtracting the product of the virtual impedance and the output current from the no-load voltage, the virtual impedance performs a role equivalent to an actual impedance. The distinct feature of control law (3) is that the command is generated using only local information that is easily accessible from each power source. In other words, the output of different power sources can be coordinated without requiring communication with the central PCU.

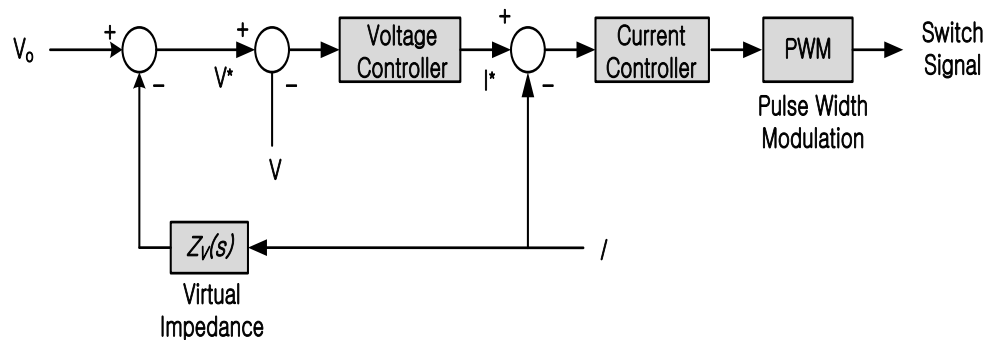


Figure 6. Block diagram of a virtual impedance-based power management.

The effect of virtual impedance to the power sharing ratio can be studied using the equivalent circuit of a dc EPS as shown in Figure 7. As shown in Figure 7, the EPS consists of two sources, a common load, the cable impedance and the virtual impedance. The relationship between the output current of each source and the load current can be written as

$$I_{load}(s) = I_{o1}(s) + I_{o2}(s) \quad (4)$$

where I_{load} is the total load current, I_{o1} is the output current of source 1 and I_{o2} is the output current of source 2. Because the output current of each source is determined by the impedance between each source and the load, the output current of each source can be written as [52]

$$I_{o1}(s) = \frac{[R_L + Z_{v2}(s) + Z_{c2}(s)]V_{o1}(s) - R_L V_2(s)}{[Z_{v1}(s) + Z_{c1}(s)][Z_{v2}(s) + Z_{c2}(s)] + R_L[Z_{v1}(s) + Z_{c1}(s) + Z_{v1}(s) + Z_{c1}(s)]} \quad (5)$$

$$I_{o2}(s) = \frac{[R_L + Z_{v1}(s) + Z_{c1}(s)]V_{o2}(s) - R_L V_1(s)}{[Z_{v1}(s) + Z_{c1}(s)][Z_{v2}(s) + Z_{c2}(s)] + R_L[Z_{v1}(s) + Z_{c1}(s) + Z_{v1}(s) + Z_{c1}(s)]} \quad (6)$$

where R_L is the load resistance, V_k , Z_{vk} , Z_{ck} , is the no load output voltage, virtual impedance and cable impedance of power source k ($k = 1, 2$), respectively.

As the no-load voltages of power sources that are connected in parallel to a common bus are typically set to an identical value (i.e., $V_{o1} = V_{o2}$), the power sharing ratio between the two sources can be written as

$$\frac{I_{o1}(s)}{I_{o2}(s)} = \frac{Z_{v2}(s) + Z_{c2}(s)}{Z_{v1}(s) + Z_{c1}(s)} = \frac{Z_{v2}(s) + R_{c2} + sL_{c2}}{Z_{v1}(s) + R_{c1} + sL_{c1}} \quad (7)$$

where R_{ck} and L_{ck} are the cable resistance and inductance of power source k , respectively. As shown in Equation (7), the current sharing ratio between the power sources is determined by the parameter values of the virtual impedance and the cable impedance. When the virtual impedance is designed to be purely resistive and the values are sufficiently larger than the cable resistance ($R_{v1}, R_{v2} \gg R_{c1}, R_{c2}$), the power sharing ratio between the two sources at steady state is determined by the virtual resistance value. Although selecting a large virtual resistance value would contribute to achieving satisfactory power sharing performance at steady state by decreasing the effect of cable resistance [53], a larger bus voltage deviation would occur as a result of a larger decrease in the voltage reference command. In case the wiring has a large inductance value, furthermore, the load sharing ratio during transients would be highly affected by the cable characteristics rather than the designed virtual resistance value. Hence, the virtual resistance approach would show limited effectiveness for achieving satisfactory load sharing performance during transients. In case of aircrafts, power transients could occur because of dynamic flight patterns, operation mode transitions and activation of pulsed power loads. In order to address such limitations of the purely resistive virtual impedance configuration and the occurrence of frequent power transients in aircrafts, this research considers an alternative virtual impedance configuration by using a virtual inductance as follows.

3.3. Virtual Inductance Based Power Management

In this research, the virtual impedance that includes not only a resistive term but also an inductive term is considered. That is, the overall command of the power source is generated as

$$V_i^*(s) = V_0(s) - (R_v + sL_v) \cdot I(s) \quad (8)$$

where R_v is the virtual resistance and L_v is the virtual inductance. Since the virtual impedance includes a frequency dependent term (sL_v), the dynamic response of the voltage command is expected to be different from the case of a purely resistive virtual impedance ($L_v = 0$) during transients. In order to study the effect of the virtual inductance, the response characteristics of power sources with different types of virtual impedances are considered. For the network of Figure 7, it is assumed that the virtual

impedances of the two sources are configured to be different so that a virtual inductance is included for power source #2 only. In other words, the virtual impedances of the two power sources were configured as

$$Z_{v1}(s) = R_v \tag{9}$$

$$Z_{v2}(s) = R_v + sL_v \tag{10}$$

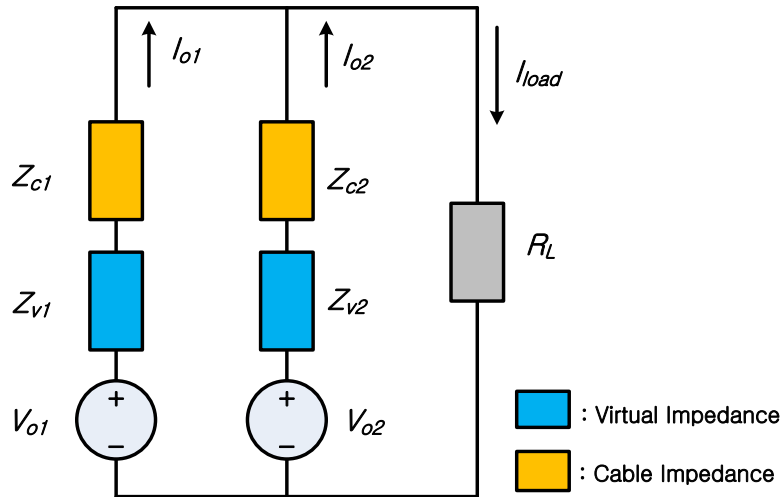


Figure 7. Equivalent circuit of an EPS with two sources connected in parallel.

For the considered virtual impedance configuration, the output current response of the two power sources to a load current change can be described by the transfer functions written as

$$M_1(s) = \frac{I_{o1}(s)}{I_o(s)} = \frac{Z_{v2}(s) + Z_{c2}(s)}{\Delta(s)} = \frac{(L_v + L_c)s + (R_v + R_c)}{\Delta(s)} \tag{11}$$

$$M_2(s) = \frac{I_{o2}(s)}{I_o(s)} = \frac{Z_{v1}(s) + Z_{c1}(s)}{\Delta(s)} = \frac{L_c s + (R_v + R_c)}{\Delta(s)} \tag{12}$$

where $\Delta(s) = (L_v + 2L_c)s + 2R_v + 2R_c$, $R_c = R_{c1} = R_{c2}$ is the cable resistance, $L_c = L_{c1} = L_{c2}$ is the cable inductance, M_1 is the transfer function between the load current and output current of source 1, and M_2 is the transfer function between the load current and output current of source 2. Since the output current of the two sources for a given load change responds according to (11) and (12), the power sharing ratio between the two sources at steady state and during transients can be determined from M_1 and M_2 . Figure 8 shows how the magnitude of the M_1 and M_2 varies at different frequency ranges using the parameter values of $R_v = 50 \text{ m}\Omega$, $L_v = 1 \text{ mH}$, $L_c = 50 \text{ }\mu\text{H}$, and $R_c = 10 \text{ m}\Omega$.

As shown in Figure 8, the response characteristics of the power sources changes depending on the frequency range. While the magnitudes of the two transfer functions are similar at low frequencies, an apparent difference can be observed at higher frequencies. Such a difference can be explained by the increased impedance magnitude at higher frequencies which is caused by the virtual inductance.

In the considered case, for instance, most of the power transients would be handled by the power source which has a purely resistive virtual impedance. While the virtual resistance value affects the steady state power sharing ratio, the virtual inductance value determines the performance during transient states.

The effect of a virtual inductance to the power sharing ratio could also be explained from the fact that the output current of each source is determined by the effective impedance between each source and the common load [54]. In case an identical virtual resistance value is considered for both sources and only source 2 includes a virtual inductance, it is evident that the effective impedance

seen from the load at non-zero frequencies would be larger for source 2 than source 1. Hence, most of the transient power demand would be supplied by source 1 that is connected to the load through a smaller impedance.

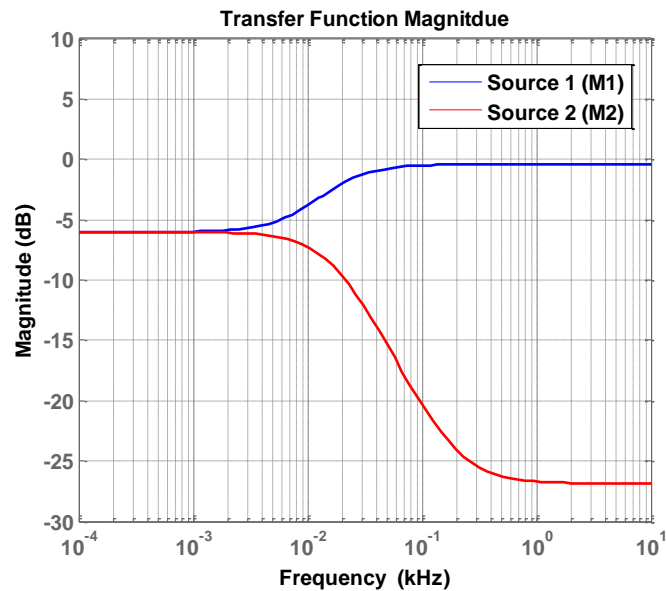


Figure 8. Frequency response of transfer functions for source 1 and source 2.

Similar to other droop-based approaches [15,38], a deviation in the main bus voltage would occur as a result of the voltage drop caused by the virtual resistance. While several approaches that apply an additional voltage restoration control loop have been reported for stationary microgrid applications [38,39], it is worth reviewing alternative approaches to handle such a voltage drop issue in aircrafts. For example, direct connection of the battery to the electrical bus [27] (which has also been applied in telecommunication systems [55]) would not only address the voltage drop but also enable immediate response of the battery when all primary power sources are lost. Such a solution would also handle stability issues that could occur with increased connection of constant power loads [27]. Selecting the virtual resistance value according to the range of a normal voltage according to design standards could also be considered as in previous studies for aircrafts [41]. According to MIL-STD-704F [56], which specifies EPS characteristics for aircrafts, the steady-state voltage range during normal operation is given as 250–280 V for a 270 V dc system and 22–29 V for a 28 V dc system. Connecting more droop-controlled sources in parallel to the electrical bus would also contribute to voltage drop minimization [37]. Since past research has focused on development of control approaches to mitigate the droop originated voltage drop, this research focuses on realizing decentralized power sharing using the virtual inductance with a particular focus on transient periods. Details on implementation examples of voltage restoration controllers can be referred from [38,39].

3.4. Effectiveness of the Proposed Approach for MEA Applications

For MEA platforms, the considered control approach can be used to realize flexible power management among different power sources. The power sharing ratio can be set to be different between steady state and transient periods through effective use of a virtual inductance. Such a feature contributes to stable operation of EPSs in aircrafts by enabling power management of various sources according to their energy density and power density. Considering the increased use of multi-source EPSs in MEA [7,24], it is necessary that the power output of different sources is properly coordinated to meet the load demand during the overall flight profile. In particular, the power flow should be controlled so that each source operates according to its own power density and energy density characteristics. For instance, the EPS could be managed such that the source with a large power density

handles most of the power transients, while the source with superior energy density supplies most of the power during steady state. According to such an operation scenario, the power sharing ratio should be different depending on the load demand profile (i.e., steady state and transient). The importance of managing the output of power sources during transients could also be highlighted from aging characteristics of power sources. In case of a fuel cell, which has been considered as a main power source for various vehicular platforms [7,24], it has been reported that the lifetime is highly affected by the frequency and level of power transients that the fuel cell experiences during its operation [48].

By applying the considered power management approach, the power sharing ratio can be adjusted in a flexible manner by shaping the virtual impedance of each source. In details, the virtual resistance is determined according to the desired power sharing ratio at steady state, while the virtual inductance can be used to adjust the output characteristics during transients only. For the EPS of Figure 7, for example, consider the case when the virtual impedance and the cable impedance parameters are set as $R_{v1} = 50 \text{ m}\Omega$, $L_{v1} = 0$, $R_{v2} = 25 \text{ m}\Omega$, $L_{v2} = 1 \text{ mH}$, $R_{c1} = R_{c2} = 10 \text{ m}\Omega$, $L_{c1} = L_{c2} = 50 \text{ }\mu\text{H}$. According to such parameter values, the output impedance frequency characteristics of the two sources can be plotted as Figure 9. It should be noted that the virtual resistance value of source 2 is smaller than that of source 1. Hence, source 2 supplies more power than source 1 at steady state. However, a virtual inductance of 1mH is implemented only in source 2, and the magnitude of the overall impedance at higher frequencies of source 1 is smaller than that of source 2. Hence, source 2 supplies more power than source 1 at steady state and source 1 handles most of the transient power than source 2.

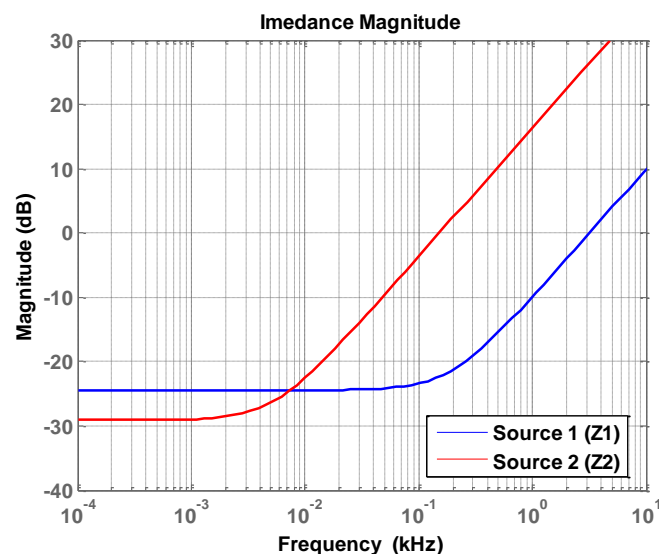


Figure 9. Frequency characteristics of impedances for source 1 and source 2.

Although a similar effect can be achieved by a centralized control approach, it should be highlighted that the power sharing at both transient and steady state can be accomplished by simply designing the virtual impedance of each power source control law in a decentralized manner. For an EPS that consists of sources that have different power density levels, for example, it is possible to let the source with the highest power density to handle most of the power transients by designing the virtual impedance. While the source with the largest power density would be configured to have a purely resistive virtual impedance, the response of the rest of the sources to a load change could be delayed by adopting a virtual impedance that includes both a resistive and an inductive term. Through such control, it is possible to prevent operation cases where the source fails to meet sudden load power changes because of its inherent slow dynamics.

4. Verification Results

The performance of the considered power control approach was verified by a simulation study. Figure 10 shows the configuration of the simulated EPS. As shown in Figure 10, the system uses 270 V dc as the main bus and consists of two sources, cable wiring, and loads. In order to perform power conversion, each power source is connected to the system bus through a buck converter. Detailed parameter values of the simulated system are given in Table 1.

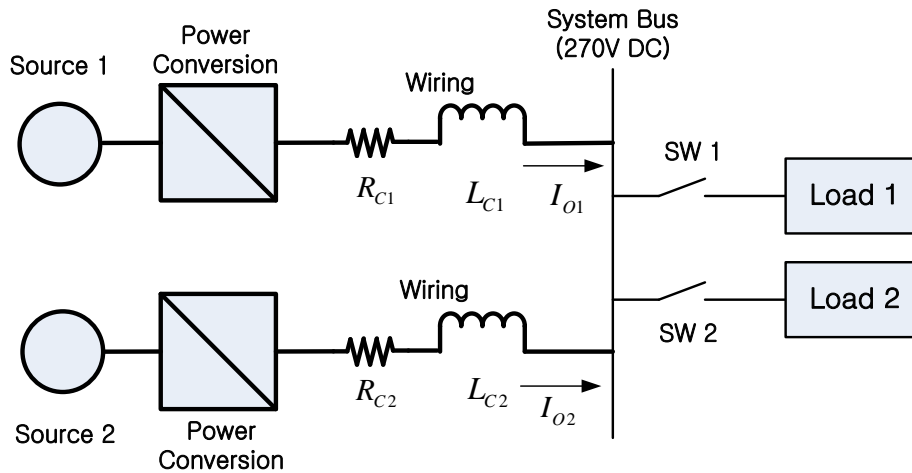


Figure 10. Configuration of the simulated EPS.

Table 1. Parameter values used for simulation.

System Parameter	Value
Converter Switching Frequency	20 kHz
Converter Inductance	1 mH
Converter Capacitance	1 mF
Source Output Voltage	500 V
Cable Resistance	$R_c = 10 \text{ m}\Omega$
Cable Inductance	$L_c = 50 \text{ }\mu\text{H}$

In order to study the effect of a virtual inductance to the power sharing performance, the virtual impedance configuration of each source was set to be different from each other. While the virtual impedance of source 1 was configured to be purely resistance ($R_{v1} = 50 \text{ m}\Omega$ and $L_{v1} = 0$), the virtual impedance of source 2 was configured to include both a virtual resistance and a virtual inductance ($R_{v2} = 50 \text{ m}\Omega$ and $L_{v2} = 1 \text{ mH}$). Figure 11 shows the output current of the two sources when the load power was increased from 7.29 kW to 14.58 kW at $t = 0.5 \text{ s}$. The difference between the two-output current is also plotted for comparison purposes. As the virtual resistance value is set to the same value, the differences of the output current between both sources are negligible at steady state. However, a noticeable difference is observed during the transient period. It could be seen that the source 1 (i.e., source with a purely resistive virtual impedance) supplies most of the power compared to source 2. During transients, as shown in Figure 11, instants that the power output of source 1 is 1.8 times larger than that of source 2 is observed. Hence, the output of power sources during transients could be managed by the virtual impedance design. When the transient output of a certain source should be limited, for example, the virtual inductance could be effectively used to shape the transient response. The total load current and the bus voltage for the case of Figure 11 are shown in Figure 12. While the bus voltage experiences a transient undershoot as soon as the load is increased at $t = 0.5 \text{ s}$, it could be seen that the bus voltage satisfies the normal voltage range that is defined in the aircraft design standard [56]. Because of the virtual resistance, as mentioned in Section 3.4, a voltage drop that corresponds to the load power level is observed. As the amount of deviation is affected by various

system parameters (e.g., load current, virtual resistance, number of droop sources that are connected in parallel), the voltage regulation performance could be managed by adjusting such design factors.

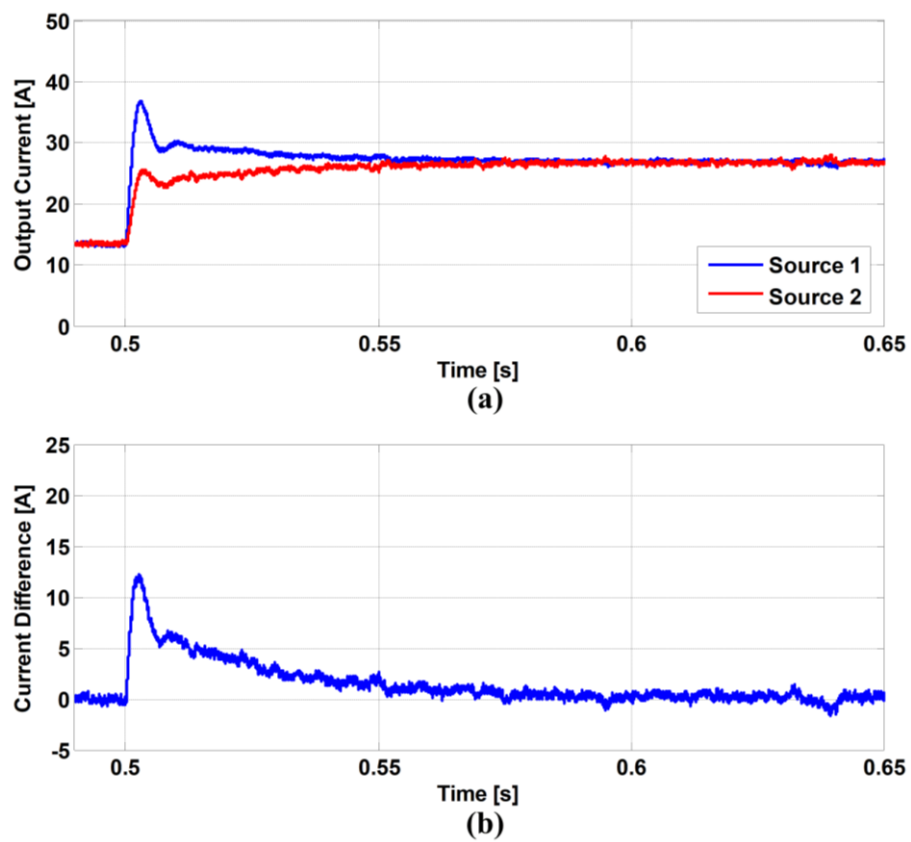


Figure 11. Simulated output current waveform ($L_{v2} = 1$ mH). (a): Output Current, (b): Difference.

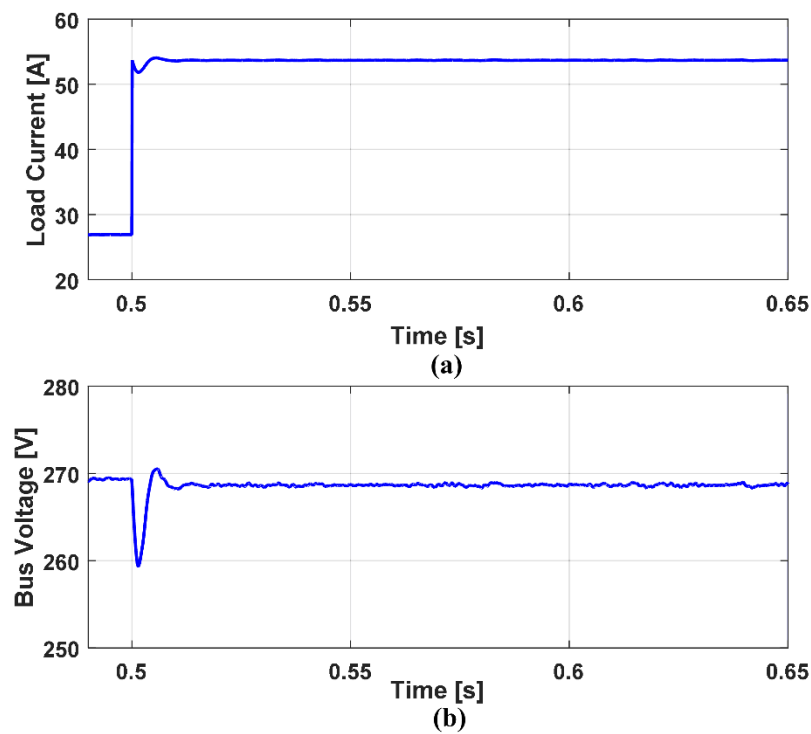


Figure 12. Simulated load current and bus voltage ($L_{v2} = 1$ mH). (a): Load Current, (b): Bus Voltage.

Figure 13 shows the waveform when a larger virtual inductance value is considered for the same EPS configuration. In this case, a virtual inductance value that is three times larger than the previous case was considered (i.e., $L_{v2} = 3$ mH). Regarding the output current at steady state, it can be seen that the output of both sources is similar. Such results can be explained by the identical virtual resistance value. By comparing the waveforms of Figures 11 and 13, it can be seen that the behavior of output current during transients is highly affected by the virtual inductance value. Because of the larger virtual inductance used in source 2, the difference of the response dynamics between the two sources has increased. As a result, the source with a purely resistive virtual impedance would supply more power during the transient period.

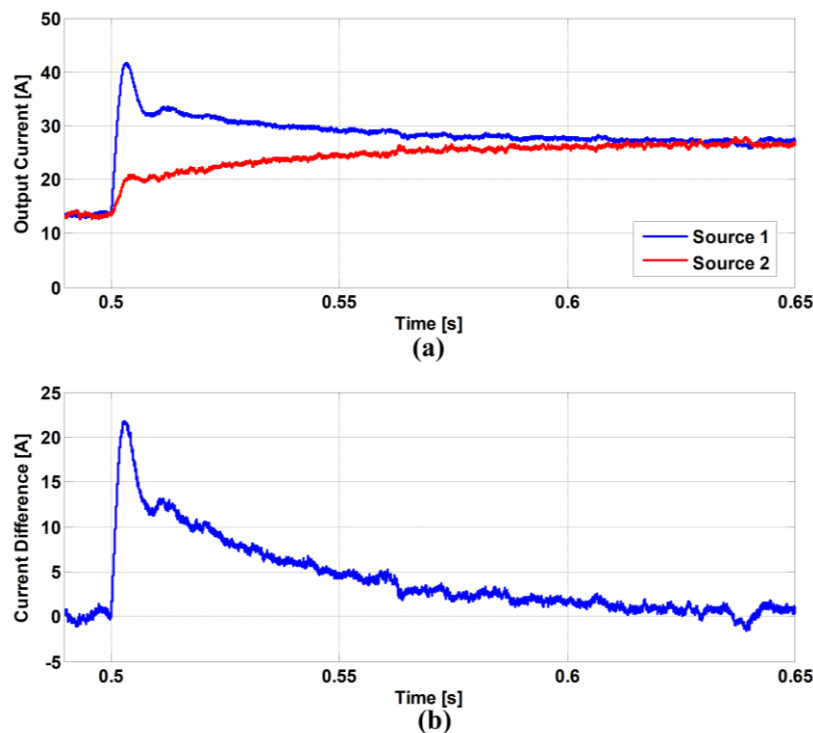


Figure 13. Simulated output current waveform ($L_{v2} = 3$ mH). (a): Output Current, (b): Difference.

Figure 14 shows that the proposed control approach can coordinate the output of power sources such that the power sharing ratio at steady state and during transients could be set to be different. Such a difference in the power sharing ratio is realized by the parameter values of the virtual impedance. In case of Figure 14, the virtual impedance values of the two sources were selected as $R_{v1} = 50$ m Ω , $L_{v1} = 0$, $R_{v2} = 25$ m Ω , and $L_{v2} = 0.1$ mH. Because of the smaller virtual resistance value, it is expected that source 2 would supply more power than source 1 at steady state. Because of the virtual inductance in source 2, however, source 1 is expected to supply most of the power during transients. In fact, Figure 14 shows such response characteristics of the output current when a load increase occurs at $t = 0.5$ s. While source 1 supplies most of the transient power, the output of source 2 is larger than that of source 1 at steady state. In case only the virtual resistance was considered for decentralized power control, it is evident that the output of source 2 (i.e., the source with smaller virtual resistance) would be larger than that of source 1 at both steady state and transient periods. However, Figure 14 demonstrates that an additional degree of freedom that enables separate control between steady state and transient performance is introduced by the virtual inductance.

Figure 15 shows the output current response when a step-up/step-down change in the load power is introduced. In order to observe the power sharing difference depending on the virtual impedance configuration, it was assumed that the virtual resistance value of source 1 is smaller than that of source 2 ($R_{v1} = 50$ m Ω , $R_{v2} = 25$ m Ω) In addition, a virtual inductance of 1 mH was considered only for

source 2. When a step increase in the load power is introduced at $t = 0.5$ s, source 1 handles most of the load demand during transients. Once the transients decay, source 2 supplies more power than source 1 according to the virtual resistance value. In addition, a similar pattern in the transient power sharing was observed when a step decrease in the load power is introduced at $t = 0.75$ s. Similar to load step up, source 1 shows a larger steeper current change rate than the output current of source 2. For the considered operation scenario, source 1 experiences a power change rate that is twice larger than that of source 2. Simultaneously, the output of source 1 at steady state is limited so that source 2 could supply more power for a longer period. From the waveforms of Figures 14 and 15, it could be seen that the power sharing characteristics in a multi-source EPS can be controlled with higher flexibility by adjusting both the virtual resistance and the virtual inductance.

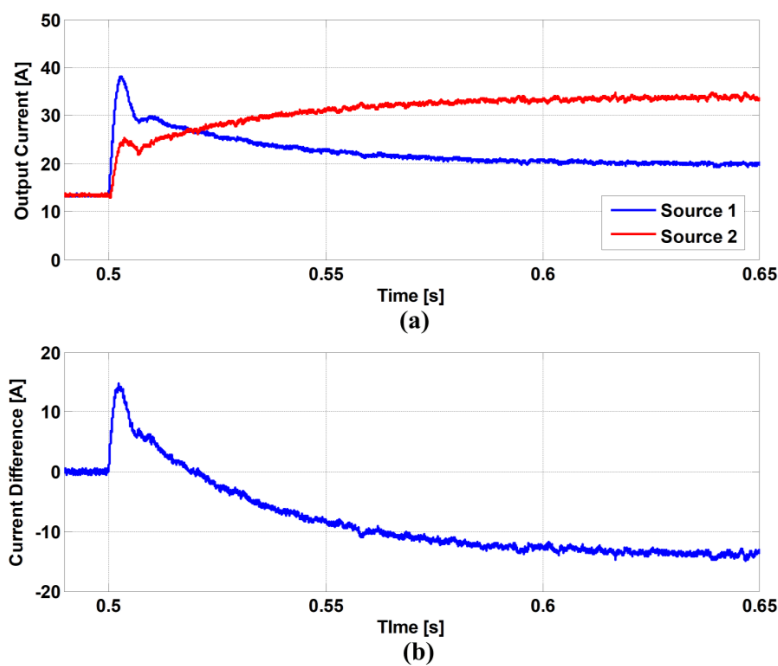


Figure 14. Simulation results with different virtual resistance values. (a): Output Current, (b): Difference.

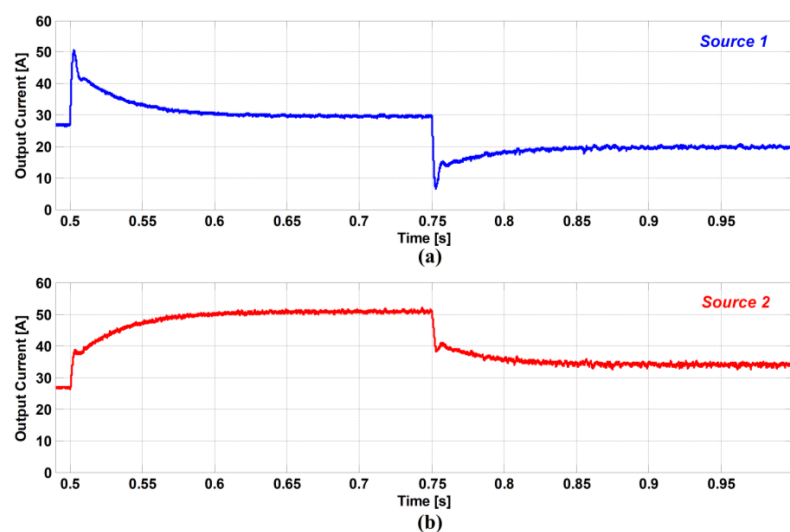


Figure 15. Simulation results of the proposed approach with step-up/step-down changes. (a): Source 1 Output Current, (b): Source 2 Output Current.

From the perspective of energy density and power density of sources, it is worth considering an EPS control approach so that high energy density sources (e.g., fuel cell and battery) operate according to the profile of source 2, while high power density sources (e.g., supercapacitor) operate similar to the profile of source 1. That is, letting power sources that are located on the lower right side of Figure 3 to handle most of the load demand during transients and assigning power sources that are located on the upper left side of Figure 3 to supply more power at steady state. It is worth noting that determining the optimal power sharing ratio at steady state and transients would be case dependent. During the design stage of an actual aircraft, in fact, the detailed data of each power source could be considered to determine which power source should handle more power during different time scales (i.e., short transients and long steady state). Examples of such data include power source type, power density, energy density, power source capacity and mission requirements.

5. Conclusions

With the increased use of electrical power to perform critical functions in the MEA, development of reliable control architectures for EPSs is necessary. This paper introduced a decentralized control approach for EPS control in MEA platforms. By using the virtual impedance, the output of different power sources can be coordinated without relying on extensive communication among EPS components. In particular, the effective use of virtual inductance for managing power sharing during transients was studied. As the virtual impedance consists of both virtual resistance and virtual inductance, the power sharing ratio could be adjusted to be different between steady state and transient periods. The effectiveness and performance of the considered control approach were also demonstrated by simulating an aircraft electrical system with different virtual impedance configurations. It was shown that the power sharing ratio during transients can be adjusted by changing the difference of the virtual inductance value. The proposed approach contributes to higher flexibility of configuration and power flow. Not only the needs for EPS configuration modification in aircrafts could be effectively addressed by the decentralized nature of the control architecture, but also the output of each power source could be managed to meet output characteristics of each source. The design of the virtual resistance and the virtual inductance could be effectively used to coordinate the power sharing ratio at both steady state and transient periods in an independent manner. Such increased flexibility would enable optimized operation of MEA by managing the output of various sources that have different power density and energy density characteristics.

Author Contributions: Formal analysis, M.K.; Literature Review, S.L.; Verification, S.B.; Writing: Draft Preparation, M.K., S.L. and S.B.; Writing: Review and Editing, S.B.

Funding: This research was supported by Basic Science Research Program through the National Research Foundation of Korea (NRF) funded by the Ministry of Education (Grant Number: 2017R1D1A1B03031723). This work was supported by the Korea Institute of Energy Technology Evaluation and Planning (KETEP) and the Ministry of Trade, Industry & Energy (MOTIE) of the Republic of Korea (No. 20161210200560).

Conflicts of Interest: The authors declare no conflict of interest.

Nomenclature

M	Total number of EPS components
R_{EPS}	Reliability of the overall EPS
R_i	Reliability of the communication link between the PCU and the i th EPS component
λ	Failure rate of the communication link
$V_{ok}; i_{ok}$	No-load voltage of the k th power source ; Output current of the k th power source
$Z_{vk}; R_{vk}; L_{vk}$	Virtual impedance; Virtual resistance; Virtual inductance of the k th power source
I_{load}	Total load current
$Z_{ck}; R_{ck}; L_{ck}$	Cable impedance; Cable resistance; Cable inductance of the k th power source
R_L	Load resistance
V_k^*	Voltage command of the k th power source

M_k	Transfer function between the load current and output current the k th power source
EPS	Electrical Power System
EMI	Electromagnetic Interference
MEA	More Electric Aircraft
PCU	Power Control Unit
PEMFC	Proton Exchange Membrane Fuel Cell
PV	Photovoltaics
PWM	Pulse Width Modulation
SOC	State-of-Charge
SOFC	Solid Oxide Fuel Cell

References

1. Un-Noor, F.; Padmanaban, S.; Mihet-Popa, L.; Mollah, M.N.; Hossain, E. A comprehensive study of key electric vehicle (EV) components, technologies, challenges, impacts, and future direction of development. *Energies* **2017**, *10*, 1217. [[CrossRef](#)]
2. Jin, Z.; Meng, L.; Guerrero, J.M.; Han, R. Hierarchical control design for a shipboard power system with DC distribution and energy storage aboard future more-electric ships. *IEEE Trans. Ind. Inform.* **2018**, *14*, 703–714. [[CrossRef](#)]
3. Sarlioglu, B.; Morris, C.T. More electric aircraft: Review, challenges, and opportunities for commercial transport aircraft. *IEEE Trans. Transp. Electrification* **2015**, *1*, 54–64. [[CrossRef](#)]
4. Ganev, E. Selecting the best electric machines for electrical power-generation systems: High-performance solutions for aerospace more electric architectures. *IEEE Electrification Mag.* **2014**, *2*, 13–22. [[CrossRef](#)]
5. Bennet, J.W.; Mecrow, B.C.; Atkinson, D.J.; Atkinson, G.J. Safety-critical design of electromechanical actuation systems in commercial aircraft. *IET Electr. Power Appl.* **2011**, *5*, 37–47. [[CrossRef](#)]
6. Neuman, T. Fly the electric skies. *IEEE Spectr.* **2016**, *53*, 44–48. [[CrossRef](#)]
7. Gong, A.; Verstraete, D. Fuel cell propulsion in small fixed-wing unmanned aerial vehicles: Current status and research needs. *Int. J. Hydrogen Energy* **2017**, *42*, 21311–21333. [[CrossRef](#)]
8. Moir, I.; Seabridge, A. *Aircraft Systems: Mechanical, Electrical, and Avionics Subsystems Integration*, 3rd ed.; Wiley: New York, NY, USA, 2008.
9. Chen, J.; Wang, C.; Chen, J. Investigation on the selection of electric power system architecture for future more electric aircraft. *IEEE Trans. Transp. Electrification* **2018**, *4*, 563–576. [[CrossRef](#)]
10. Chang, J.; Wang, A. New VF-power system architecture and evaluation for future aircraft. *IEEE Trans. Aerosp. Electron. Syst.* **2006**, *42*, 527–539. [[CrossRef](#)]
11. Areerak, K.N.; Bozhko, S.V.; Asher, G.M.; De Lillo, L.; Thomas, D.W.P. Stability study for a hybrid AC-DC more-electric aircraft power system. *IEEE Trans. Aerosp. Electron. Syst.* **2012**, *48*, 329–347. [[CrossRef](#)]
12. Roboam, X.; Sareni, B.; Andrade, A. More electricity in the air: Toward optimized electrical networks embedded in more-electrical aircraft. *IEEE Ind. Electron. Mag.* **2012**, *6*, 6–17. [[CrossRef](#)]
13. Wang, C.; Li, X.; Guo, L.; Li, Y.W. A nonlinear-disturbance-observer-based DC-bus voltage control for a hybrid AC/DC microgrid. *IEEE Trans. Power Electron.* **2014**, *29*, 6162–6177. [[CrossRef](#)]
14. Dragicevic, T.; Guerrero, J.M.; Vasquez, J.C.; Skrllec, D. Supervisory control of an adaptive-droop regulated DC microgrid with battery management capability. *IEEE Trans. Power Electron.* **2014**, *29*, 695–706. [[CrossRef](#)]
15. Dragicevic, T.; Lu, X.; Vasquez, J.C.; Guerrero, J.M. DC microgrids-Part 1: A review of control strategies and stabilization techniques. *IEEE Trans. Power Electron.* **2016**, *31*, 4876–4891. [[CrossRef](#)]
16. Tahim, A.P.N.; Pagano, D.J.; Lenz, E.; Stramosk, V. Modeling and stability analysis of islanded DC microgrids under droop control. *IEEE Trans. Power Electron.* **2015**, *30*, 4597–4607. [[CrossRef](#)]
17. Gu, Y.; Li, W.; He, X. Frequency-coordinating virtual impedance for autonomous power management of DC microgrid. *IEEE Trans. Power Electron.* **2015**, *30*, 2328–2337. [[CrossRef](#)]
18. Xu, Q.; Hu, X.; Wang, P.; Xiao, J.; Tu, P.; Wen, C.; Lee, M.Y. A decentralized dynamic power sharing strategy for hybrid energy storage system in autonomous DC microgrid. *IEEE Trans. Ind. Electron.* **2017**, *64*, 5930–5941. [[CrossRef](#)]

19. Zhao, X.; Li, Y.W.; Tian, H.; Wu, X. Energy management strategy of multiple supercapacitors in a DC microgrid using adaptive virtual impedance. *IEEE J. Emerg. Sel. Top. Power Electron.* **2016**, *4*, 1174–1185. [[CrossRef](#)]
20. Ou, T.; Li, K.; Huang, C. Improvement of transient stability in a hybrid power multi-system using a designed NIDC (Novel Intelligent Damping Controller). *Energies* **2017**, *10*, 488. [[CrossRef](#)]
21. Ou, T.; Hong, C. Dynamic operation and control of microgrid hybrid power systems. *Energy* **2014**, *66*, 314–323. [[CrossRef](#)]
22. Motapon, S.N.; Dessaint, L.A.; Al-Haddad, K. A comprehensive study of energy management schemes for a fuel-cell hybrid emergency power system of more-electric aircraft. *IEEE Trans. Ind. Electron.* **2014**, *61*, 1320–1334. [[CrossRef](#)]
23. Zhang, F.; Mollet, F.; Saudemont, C.; Robyns, B. Experimental validation of energy storage system management strategies for a local DC distribution system of more electric aircraft. *IEEE Trans. Ind. Electron.* **2010**, *57*, 3905–3916. [[CrossRef](#)]
24. Lee, B.; Kwon, S.; Park, P.; Kim, K. Active power management system for an unmanned aerial vehicle powered by solar cells, a fuel cell, and batteries. *IEEE Trans. Aerosp. Electron. Syst.* **2014**, *50*, 3167–3177. [[CrossRef](#)]
25. Ou, T. A novel unsymmetrical fault analysis for microgrid distribution systems. *Electr. Power Energy Syst.* **2012**, *43*, 1017–1024. [[CrossRef](#)]
26. Ou, T. Ground fault current analysis with a direct building algorithm for microgrid distribution. *Electr. Power Energy Syst.* **2013**, *53*, 867–875. [[CrossRef](#)]
27. Kwasinski, A.; Onwuchekwa, C.N. Dynamic behavior and stabilization of DC microgrids with instantaneous constant-power loads. *IEEE Trans. Power Electron.* **2011**, *26*, 822–834. [[CrossRef](#)]
28. Lim, J.; Kim, H.; Cho, K.; Bae, J. Stand-alone microgrid inverter controller design for nonlinear, unbalanced load with output transformer. *Electronics* **2018**, *7*, 55. [[CrossRef](#)]
29. Lei, T.; Wu, C.; Liu, X. Multi-objective optimization control for the aerospace dual-active bridge power converter. *Energies* **2018**, *11*, 1168. [[CrossRef](#)]
30. Onambele, C.; Elsied, M.; Mpanda Mabwe, A.; El Hajjaji, A. Multi-phase modular drive system: A case study in electrical aircraft applications. *Energies* **2018**, *11*, 5. [[CrossRef](#)]
31. Burgos, R.; Chen, G.; Wang, F.; Boroyevich, D.; Odendaal, W.G.; Van Wyk, J.D. Reliability-oriented design of three-phase converters for aircraft applications. *IEEE Trans. Aerosp. Electron. Syst.* **2012**, *48*, 1249–1263. [[CrossRef](#)]
32. Muller, J.-K.; Mertens, A. Power electronics design for a direct-driven turbo compressor used as advanced high-lift system in future aircraft. In Proceedings of the 43rd Annual Conference of the IEEE Industrial Electronics Society, Beijing, China, 29 October–1 November 2017; pp. 1–6.
33. Zhai, L.; Zhang, T.; Cao, Y.; Yang, S.; Kavuma, S.; Feng, H. Conducted EMI prediction and mitigation strategy based on transfer function for a high-low voltage DC-DC converter in electric vehicle. *Energies* **2018**, *11*, 1028. [[CrossRef](#)]
34. Giglia, G.; Ala, G.; Piazza, M.C.D.; Giaconia, G.C.; Luna, M.; Vitale, G.; Zanchetta, P. Automatic EMI filter design for power electronic converters oriented to high power density. *Electronics* **2018**, *7*, 9. [[CrossRef](#)]
35. Henke, M.; Narjes, G.; Hoffmann, J.; Wohlers, C.; Urbanek, S.; Heister, C.; Steinbrink, J.; Canders, W.R.; Ponick, B. Challenges and opportunities of very light high-performance electric drives for aviation. *Energies* **2018**, *11*, 344. [[CrossRef](#)]
36. Diaz, N.L.; Luna, A.C.; Vasquez, J.C.; Guerrero, J.M. Centralized control architecture for coordination of distributed renewable generation and energy storage in islanded AC microgrids. *IEEE Trans. Power Electron.* **2017**, *32*, 5202–5213. [[CrossRef](#)]
37. Gao, F.; Bozhko, S.; Costabeber, A.; Asher, G.; Wheeler, P. Control design and voltage stability analysis of a droop-controlled electrical power system for more electric aircraft. *IEEE Trans. Ind. Electron.* **2017**, *64*, 9271–9281. [[CrossRef](#)]
38. Kim, M.; Kwasinski, A. Decentralized hierarchical control of active power distribution nodes. *IEEE Trans. Energy Convers.* **2014**, *24*, 934–943. [[CrossRef](#)]
39. Guerrero, J.M.; Vasquez, J.C.; Matas, J.; de Vicuna, L.G.; Castilla, M. Hierarchical control of droop-controlled AC and DC microgrids-A general approach toward standardization. *IEEE Trans. Ind. Electron.* **2011**, *58*, 158–172. [[CrossRef](#)]

40. Aten, M.; Towers, G.; Whitley, C.; Wheeler, P.; Clare, J.; Bradley, K. Reliability comparison of matrix and other converter topologies. *IEEE Trans. Aerosp. Electron. Syst.* **2006**, *42*, 867–875. [[CrossRef](#)]
41. Gao, F.; Bozhko, S.; Asher, G.; Wheeler, P.; Patel, C. An improved voltage compensation approach in a droop-controlled DC power system for the more electric aircraft. *IEEE Trans. Power Electron.* **2016**, *31*, 7369–7383. [[CrossRef](#)]
42. Yassine, M.; Fabris, D. Performance of commercially available supercapacitors. *Energies* **2017**, *10*, 1340. [[CrossRef](#)]
43. Jayasinghe, S.G.; Meegahapola, L.; Fernando, N.; Jin, Z.; Guerrero, J.M. Review of ship microgrids: System architectures, storage technologies and power quality aspects. *Inventions* **2017**, *2*, 4. [[CrossRef](#)]
44. Gonzalez-Espasandin, O.; Leo, T.J.; Navarro-Arevalo, E. Fuel cells: A real option for unmanned aerial vehicles propulsion. *Sci. World J.* **2014**, *2014*, 497642. [[CrossRef](#)] [[PubMed](#)]
45. Gao, L.; Liu, Y.; Ren, H.; Guerrero, J.M. A DC microgrid coordinated control strategy based on integrator current-sharing. *Energies* **2017**, *10*, 1116. [[CrossRef](#)]
46. Liu, Y.; Wang, J.; Li, N.; Fu, Y.; Ji, Y. Enhanced load power sharing accuracy in droop-controlled DC microgrids with both mesh and radial configurations. *Energies* **2015**, *8*, 3591–3605. [[CrossRef](#)]
47. Hamzeh, M.; Ghafouri, M.; Karimi, H.; Sheshyekani, K.; Guerrero, J.M. Power oscillations damping in DC microgrids. *IEEE Trans. Energy Convers.* **2016**, *31*, 970–980. [[CrossRef](#)]
48. Fletcher, T.; Thring, R.; Watkinson, M. An energy management strategy to concurrently optimize fuel consumption & PEM fuel cell lifetime in a hybrid vehicle. *Int. J. Hydrogen Energy* **2016**, *41*, 21503–21515.
49. Bolborici, V.; Dawson, F.P.; Lian, K.K. Hybrid energy storage systems: Connecting batteries in parallel with ultracapacitors for high higher power density. *IEEE Ind. Appl. Mag.* **2014**, *20*, 31–40. [[CrossRef](#)]
50. Rausand, R.; Holyland, A. *System Reliability Theory: Models, Statistical Methods, and Applications*, 2nd ed.; Wiley-Interscience: Hoboken, NJ, USA, 2004.
51. Erickson, R.W.; Maksimovic, D. *Fundamentals of Power Electronics*, 2nd ed.; Springer: New York, NY, USA, 2001.
52. Augustine, S.; Lakshminarasamma, N.; Mishra, M.K. Control of photovoltaic-based low-voltage DC microgrid system for power sharing with modified droop algorithm. *IET Power Electron.* **2016**, *9*, 1132–1143. [[CrossRef](#)]
53. Lu, X.; Guerrero, J.M.; Sun, K.; Vasquez, J.C. An improved droop control for DC microgrids based on low bandwidth communication with DC bus voltage restoration and enhanced current sharing accuracy. *IEEE Trans. Power Electron.* **2014**, *29*, 1800–1812. [[CrossRef](#)]
54. Paquette, A.D.; Reno, M.J.; Harley, R.G.; Divan, D.M. Sharing transient loads: Causes of unequal transient load sharing in islanded microgrid operation. *IEEE Ind. Appl. Mag.* **2014**, *20*, 23–34. [[CrossRef](#)]
55. Gadoura, I.; Grigore, V.; Hatonen, J.; Kyyra, J.; Vallittu, P.; Suntio, T. Stabilizing a telecom power supply feeding a constant power load. In Proceedings of the 20th International Telecommunications Energy Conference (INTELEC), San Francisco, CA, USA, 4–8 October 1998; pp. 243–248.
56. Aircraft Electric Power Characteristics. Available online: <http://u.dianyuan.com/upload/space/2012/04/06/1333690328-628697.pdf> (accessed on 16 July 2018).

